

# Pervasive Axonal Transport Deficits in Multiple Sclerosis Models

Catherine Diamante Sorbara,<sup>1,2</sup> Naomi Elizabeth Wagner,<sup>1</sup> Anne Ladwig,<sup>1</sup> Ivana Nikić,<sup>1</sup> Doron Merkler,<sup>3,4,5</sup> Tatjana Kleele,<sup>2</sup> Petar Marinković,<sup>2</sup> Ronald Naumann,<sup>6</sup> Leanne Godinho,<sup>2</sup> Florence Martine Baireyre,<sup>1,7</sup> Derron Bishop,<sup>8</sup> Thomas Misgeld,<sup>2,7,9,10,11,\*</sup> and Martin Kerschensteiner<sup>1,7,11,\*</sup>

<sup>1</sup>Institute of Clinical Neuroimmunology, Ludwig-Maximilians Universität München, Marchioninistraße 17, 81377 Munich, Germany

<sup>2</sup>Institute of Neuronal Cell Biology, Technische Universität München, Biedersteiner Straße 29, 80802 Munich, Germany

<sup>3</sup>Department of Pathology and Immunology, University of Geneva, Rue Michel Servet 1, 1211 Geneva, Switzerland

<sup>4</sup>Division of Clinical Pathology, Geneva University Hospital, Rue Gabrielle-Perret-Gentil 4, 1205 Geneva, Switzerland

<sup>5</sup>Department of Neuropathology, Georg-August-Universität Göttingen, Robert-Koch-Str. 40, 37099 Göttingen, Germany

<sup>6</sup>Transgenic Core Facility, Max-Planck-Institute of Molecular Cell Biology and Genetics, Pfotenhauerstraße 108, 01307 Dresden, Germany

<sup>7</sup>Munich Cluster of Systems Neurology (SyNergy), Feodor-Lynen-Straße 17, 81377 Munich, Germany

<sup>8</sup>Department of Physiology, Indiana University School of Medicine-Muncie, Cooper Science Building, CL 215, Muncie, IN 47306, USA

<sup>9</sup>German Center for Neurodegenerative Diseases (DZNE), Feodor-Lynen Straße 17, 81377 Munich, Germany

<sup>10</sup>Center of Integrated Protein Science (CIPSM), Butenandtstraße 5-13, 81377 Munich, Germany

<sup>11</sup>Co-senior author

\*Correspondence: [thomas.misgeld@lrz.tu-muenchen.de](mailto:thomas.misgeld@lrz.tu-muenchen.de) (T.M.), [martin.kerschensteiner@med.uni-muenchen.de](mailto:martin.kerschensteiner@med.uni-muenchen.de) (M.K.)

<http://dx.doi.org/10.1016/j.neuron.2014.11.006>

## SUMMARY

Impaired axonal transport can contribute to axon degeneration and has been described in many neurodegenerative diseases. Multiple sclerosis (MS) is a common neuroinflammatory disease, which is characterized by progressive axon degeneration—whether, when, and how axonal transport is affected in this condition is unknown. Here we used *in vivo* two-photon imaging to directly assay transport of organelles and the stability of microtubule tracks in individual spinal axons in mouse models of MS. We found widespread transport deficits, which preceded structural alterations of axons, cargos, or microtubules and could be reversed by acute anti-inflammatory interventions or redox scavenging. Our study shows that acute neuroinflammation induces a pervasive state of reversible axonal dysfunction, which coincides with acute disease symptoms. Moreover, perpetuated transport dysfunction, as we found in a model of progressive MS, led to reduced distal organelle supply and could thus contribute to axonal dystrophy in advanced stages of the disease.

## INTRODUCTION

Multiple sclerosis (MS) is an inflammatory disease of the CNS and a frequent cause of neurological disability. In MS, chronic disability is due to progressive axon degeneration (Trapp and Nave, 2008). During the initial phase of the disease, axon degeneration predominantly occurs in focal white matter lesions, while in later stages of the disease, a more widespread pattern of axonal pathology emerges (Lassmann et al., 2012). Such diffuse axon

degeneration is reminiscent of the continuous decline observed in classical neurodegenerative diseases, but the mechanisms that cause progressive axon loss in MS remain poorly understood. Axonal transport, which shuttles critical cell body-derived cargos back and forth between soma, axon, and synapses (Coleman, 2005; Millecamps and Julien, 2013), appears to be a vulnerable target in neuronal homeostasis. Indeed, impairments of axonal transport have been associated with axon degeneration in neurological disease. First, transport disturbances have been described in several neurodegenerative conditions and appear to precede the initiation of overt neurodegeneration (Millecamps and Julien, 2013). Second, mutations that cause neuronal and axonal degeneration in mice and humans often affect axonal transport (Baloh et al., 2007; Ebbing et al., 2008) and, in converse, mutations that affect transport can cause axon degeneration (Hurd and Saxton, 1996; LaMonte et al., 2002). Finally, therapeutic strategies that restore transport tracks and reverse transport deficits have been shown to slow the progression of axon degeneration, for example, in models of Charcot-Marie-Tooth disease or hereditary spastic paraplegia (d'Ydewalle et al., 2011; Denton et al., 2014).

While transport disturbances have thus been linked to classical neurodegenerative diseases, it is currently unclear whether and when similar transport deficits occur in neuroinflammatory lesions, how such deficits relate to structural axon damage, and which inflammatory mediators can impede transport. Here we use *in vivo* two-photon imaging to directly measure organelle transport and microtubule dynamics in acute and chronic mouse models of MS. Remarkably, we found that in neuroinflammatory lesions axonal transport was not only reduced in morphologically altered axons, but also in the majority of normal-appearing axons. Further analysis showed that transport impairments are already present before demyelination or major abnormalities of microtubule tracks became apparent. This indicates that transport deficits represent an early and pervasive stage of axonal dysfunction. Transport deficits recovered within days in an acute MS model but failed to resolve in a chronic model, resulting in a

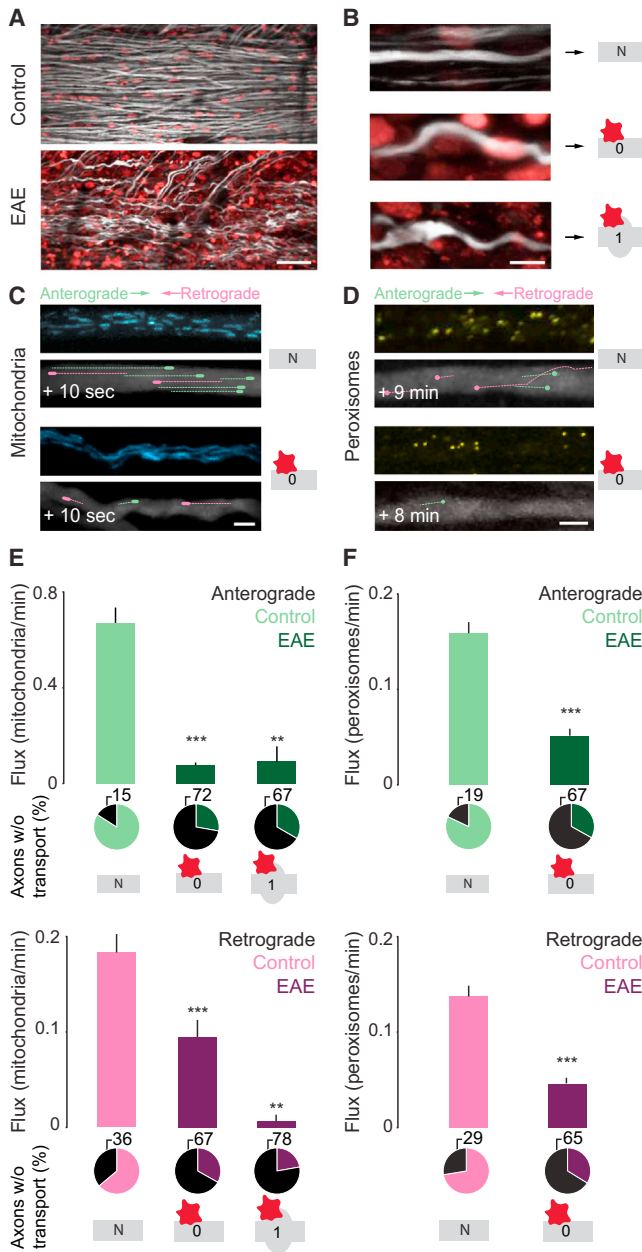


**Figure 1. In Vivo Imaging of Organelle Transport in Neuroinflammatory Lesions**

(A) In vivo two-photon image of the spinal cord of a control *Thy1-YFP-16* × *Thy1-MitoCFP-P* mouse (top) and a *Thy1-YFP-16* × *Thy1-MitoCFP-P* mouse 2 days after onset of EAE (bottom; axons, white; nuclei labeled by in vivo application of Nuclear-ID Red, red; mitochondrial channel not shown). (B) Magnified views of axons from neuroinflammatory lesions illustrating different stages of axon morphology (N, axon from a control mouse; stage 0, normal-appearing axon within an inflammatory lesion; stage 1, swollen axon within an inflammatory lesion; corresponding symbols as shown on the right are used throughout the figures). (C and D) In vivo two-photon time-lapse images of control axons (top) and stage 0 axons imaged 2 days after onset of EAE (bottom) with moving mitochondria (C), in *Thy1-YFP-16* × *Thy1-MitoCFP-P* mice, and peroxisomes (D), in *Thy1-OPF-3* × *Thy1-PeroxiYFP-376* mice, represented as pseudo-colored overlays (lines represent tracks during the indicated time period). (E and F) Quantification of anterograde (top) and

retrograde (bottom) mean flux rate in control axons and EAE axons (imaged at 2 days after onset) for mitochondria (E) ( $n = 9$ –187 axons from 8–18 *Thy1-YFP-16* × *Thy1-MitoCFP-P* mice per group; flux compared to control axons by Kruskal-Wallis test followed by Dunn's Multiple Comparison test) and peroxisomes (F) ( $n = 153$ –157 axons from 6 *Thy1-XFP* × *Thy1-PeroxiYFP* mice per group; flux compared to control axons by Mann-Whitney test). Pie charts represent the percentage of axons at each stage where no transport was seen (black slice, percentage indicated above). Scale bars represent 50  $\mu\text{m}$  in (A), 10  $\mu\text{m}$  in (B), and 5  $\mu\text{m}$  in (C) and (D). All graphs show mean + SEM; \*\*\* $p < 0.001$ .

## RESULTS

### Widespread Deficits of Organelle Transport Are Observed in Multiple Sclerosis Models

To investigate how organelle transport is affected by neuroinflammation, we used an acute experimental autoimmune encephalomyelitis (EAE) model of MS, in which inflammatory lesions with axon damage evolve in the spinal cord of mice (Figures 1A and 1B). We then established a spinal in vivo two-photon imaging approach (Davalos et al., 2008; Nikić et al., 2011) that allowed us to follow the dynamics of individual fluorescently labeled organelle cargos, such as mitochondria (in *Thy1-MitoCFP* mice; Misgeld et al., 2007) or peroxisomes (in newly generated *Thy1-PeroxiYFP* mice), in individual spinal axons in the healthy and inflamed spinal cord (Figures 1C and 1D and Movies S1 and S2 available online). Neuroinflammatory lesions were identified in vivo by application of a nuclear dye that reveals cellular infiltration (Romanelli et al., 2013) or based on the local presence of damaged axons (see Supplemental Experimental Procedures). Our in vivo recordings showed that anterograde and retrograde transport of mitochondria and peroxisomes were markedly reduced in spinal axons that pass through these lesions (Figures 1E and 1F and Movie S1). Strikingly, transport was not only reduced in axons that were swollen and hence had entered the degeneration process (Nikić et al., 2011), but also in the majority of normal-appearing axons in the lesion area. In contrast, dorsal root axons imaged proximal to the lesion area displayed normal anterograde transport and even increased retrograde transport rates (Figure S1). In inflammatory lesions, such localized transport deficits were not only observed acutely but persisted for several weeks in a chronic EAE model (Figure S2A). These transport deficits resulted in a long-lasting reduction of net organelle delivery from the soma toward the synapses, as anterograde transport rates were more profoundly affected than retrograde ones. In the case of mitochondria, for example, parts of axons that are distal to inflamed sites lacked the supply of several hundred mitochondria per day (Figure S2B). Indeed, anterograde tracing of dorsal root ganglion (DRG) axons that pass through the inflamed spinal cord revealed that local axon collaterals within the lumbar gray matter, as well as the distal axon compartments in ascending tracts of the dorsal thoracic spinal cord, became depleted of mitochondria in a chronic (but not in an acute) EAE model (Figure S3).

retrograde (bottom) mean flux rate in control axons and EAE axons (imaged at 2 days after onset) for mitochondria (E) ( $n = 9$ –187 axons from 8–18 *Thy1-YFP-16* × *Thy1-MitoCFP-P* mice per group; flux compared to control axons by Kruskal-Wallis test followed by Dunn's Multiple Comparison test) and peroxisomes (F) ( $n = 153$ –157 axons from 6 *Thy1-XFP* × *Thy1-PeroxiYFP* mice per group; flux compared to control axons by Mann-Whitney test). Pie charts represent the percentage of axons at each stage where no transport was seen (black slice, percentage indicated above). Scale bars represent 50  $\mu\text{m}$  in (A), 10  $\mu\text{m}$  in (B), and 5  $\mu\text{m}$  in (C) and (D). All graphs show mean + SEM; \*\*\* $p < 0.001$ .

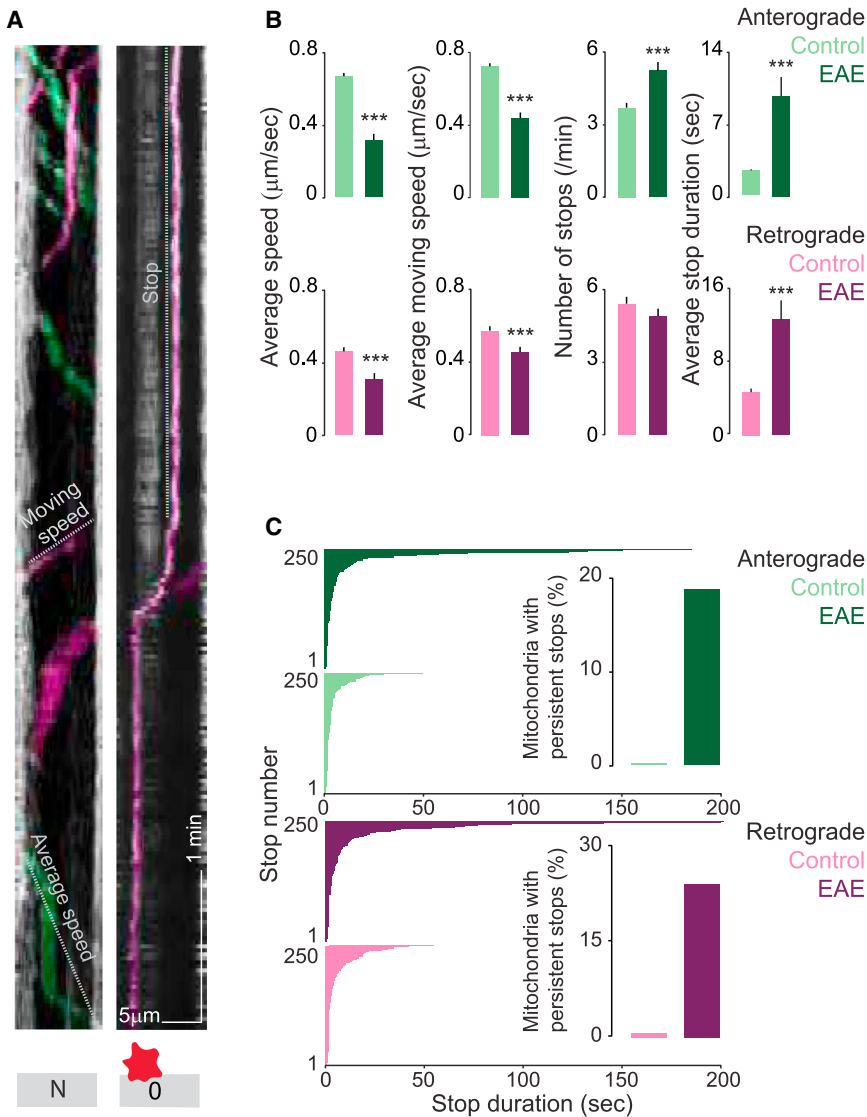


### Figure 2. Mitochondrial Stop Duration Increases in EAE Axons

(A) Kymograph of a control axon (left) and a stage 0 axon, 2 days after onset of EAE (right) in *Thy1-YFP-16 × Thy1-MitoCFP-P* mice, serving to illustrate the single mitochondrial transport characteristics that we extracted from manually tracked organelles, such as average speed, moving speed, and stopping. (B) Quantification of single mitochondrial transport characteristics ( $n = 81\text{--}454$  mitochondria,  $n = 43\text{--}100$  stage 0 axons with normally shaped mitochondria from 8–18 mice per group; compared to control axons by Mann-Whitney test). (C) Line diagram of mitochondrial stop durations taken from 250 randomly chosen stops organized from shortest (1) to longest (250). Inset shows percentage of all tracked mitochondria with persistent stops, not all displayed in line diagram. Values in (B) expressed as mean + SEM. \*\*\* $p < 0.001$ .

and 10–35 axons per group). Indeed, such organelle accumulations have also been previously documented in MS tissue (Vergo et al., 2011; Witte et al., 2009).

### Transport Deficits Precede Structural Alterations of Axons, Cargos, or Microtubule Tracks

We next asked whether focal structural alterations could explain why organelles accumulate in neuroinflammatory lesions. Demyelination or dysmyelination, for instance, have been previously shown to associate with increased organelle density in axons (Edgar et al., 2004; Kiryu-Seo et al., 2010; Ohno et al., 2014). To address the role of demyelination in vivo, we labeled myelin in the intact spinal cord using a vital dye (Romanelli et al., 2013) and measured organelle transport

To better understand why organelle transport is impaired, we tracked the movements of individual mitochondria through acute neuroinflammatory lesions in normal-appearing axons. Our results show that while parameters such as moving speed and stop frequency were only moderately altered, the duration of mitochondrial stops was dramatically increased for both anterogradely and retrogradely moving mitochondria in neuroinflammatory lesions. Furthermore, persistent arrests of organelles were almost exclusively observed in the inflamed spinal cord (Figure 2). Such persistent stops likely explain the increased density of organelles (mitochondrial density:  $0.15 \pm 0.003$  mitochondria/ $\mu\text{m}^2$  in control axons compared to  $0.25 \pm 0.008$  mitochondria/ $\mu\text{m}^2$  and  $0.35 \pm 0.02$  mitochondria/ $\mu\text{m}^2$  in normal-appearing and swollen axons within acute neuroinflammatory lesions, respectively), as well as the raised mitochondrial content (relative to control axons:  $111\% \pm 5\%$  of mitochondrial content in stage 0 axons,  $128\% \pm 9\%$  in stage 1 axons), that we observed in neuroinflammatory lesions in situ ( $n = 3\text{--}4$  *Thy1-YFP-16 × Thy1-MitoCFP-S* mice

in acute neuroinflammatory lesions. Interestingly, transport deficits were already present in myelinated axons (Figures S4A and S4B) and were thus not secondary to demyelination.

Another possibility would be that damage to mitochondria themselves, as described in neuroinflammatory lesions (Nikić et al., 2011; Witte et al., 2014), might lead to transport disruption. However, when we measured mitochondrial transport rates in intact-appearing axons with either normally shaped or morphologically altered mitochondria, we found that transport deficits preceded structural changes to organelles (Figures S4C and S4D).

Finally, we asked whether alterations of the microtubule tracks, along which organelles travel, interfere with transport. To assess the state of microtubules in individual axons at different stages of neuroinflammatory damage, we analyzed the orientation of microtubule tracks by electron microscopy (Figures 3A–3C). In addition, we evaluated the presence of post-translational modifications of tubulin, such as acetylation and

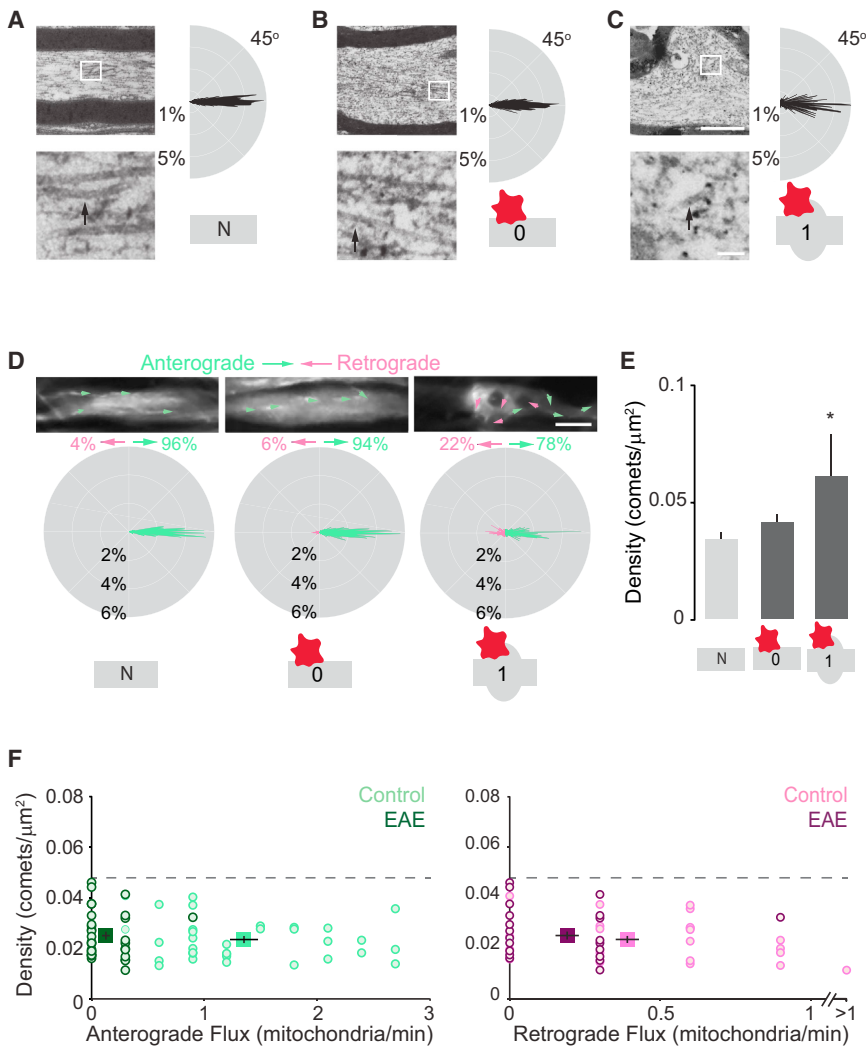


### Figure 3. Transport Deficits Occur before Marked Alterations of Microtubule Tracks

(A–C) Ultrastructural analysis of axons in the lumbar spinal cord of a control mouse (A) and a mouse perfused 2 days after onset of EAE (B), stage 0 axon; (C), stage 1 axon. Top: overview transmission electron micrographs of the axons; bottom: larger magnifications (boxed on top) illustrating microtubule morphology (arrows). Polar plots, frequency histograms with angular orientation displayed in a circle, are on the right and indicate the angle of deviation of microtubules from the corresponding axon axis (percentages on the left of the polar plot correspond to labels for the concentric rings and indicate the proportion of comets that are orientated in a given angle;  $n = 22\text{--}65$  axons from 3 mice per group). (D) In vivo two-photon assay of dynamic microtubule ends (“comets”) in control and EAE (2 days after onset) *Thy1-EB3-YFP* mice. Top: in vivo time-lapse images of axons from control and EAE (2 days after onset) *Thy1-EB3-YFP* mice (YFP, white). Comets and their directionality are highlighted by arrows (green, anterograde; pink, retrograde). Bottom: polar plots that indicate the frequencies of the angle of deviation of comets from the corresponding axon axis, as well as their directionality. Percentages of anterograde versus retrograde comets are indicated above each polar plot. Significantly fewer comets show an anterograde orientation in stage 1 EAE axons ( $78\% \pm 5\%$ ) compared to stage 0 EAE axons ( $94\% \pm 1\%$ ) and control axons ( $96\% \pm 1\%$ ;  $p < 0.001$  for stage 1 compared to stage 0 or control; Kruskal-Wallis test followed by Dunn’s Multiple Comparison test). (E) Quantification of comet density in control and EAE axons ( $n = 12\text{--}49$  axons per group from 4 control and 6 EAE mice; densities in EAE axons compared to control axons by Kruskal-Wallis test followed by Dunn’s Multiple Comparison test). (F) Quantification of both comet density and mitochondrial flux per axon are plotted derived from recordings in double-transgenic mice with differentially labeled

mitochondria and dynamic microtubule ends. Individual axons are indicated by circles with the mean of each group  $\pm$  SEM indicated by a square. A clear shift to the left within the EAE population indicates a decrease in organelle flux, while no change in comet density is apparent. Dotted gray line indicates 3 SDs from the mean comet density in control mice showing that all stage 0 axons fall within the normal distribution and do not significantly differ from control ( $n = 33$  axons per group from 4 control and 3 EAE mice). Scale bars represent 1 μm in (C), top (also for panels in A and B); 100 nm in blow-up in (C) (also for magnified details in A and B); 5 μm in (D), right (also for middle and left). Graph in (E) shows mean + SEM; graph in (F) shows mean  $\pm$  SEM for values indicated by square symbol; \* $p < 0.05$ .

tyrosination, which respectively indicate the stabilization or destabilization of microtubules (Janke, 2014), by quantitative immunohistochemistry (Figure S5). Finally, we directly assayed the density and orientation of dynamic microtubules by in vivo two-photon imaging of *Thy1-EB3-YFP* mice (Kleele et al., 2014), which express a fluorescently tagged version of the plus-end binding protein EB3 in neurons (Figures 3D–3F and Movie S3). Together, these analyses showed that transport deficits occurred in axons before marked alterations of the microtubule cytoskeleton. While there is a subset of normal appearing EAE axons, which show increased microtubule tyrosination, acetylation levels in EAE and control axons are similar, with even a slight increase seen in normal-appearing axons in EAE lesions compared to controls. Furthermore, the orientation of microtubules in electron micrographs, as well as the density and

orientation of dynamic microtubule comets, are comparable between control and normal-appearing axons in EAE. In contrast, we found disorganized, tyrosinated, and highly dynamic microtubules in a subset of swollen axons in neuroinflammatory lesions (Figures 3C–3E, Figure S5, and Movie S3). Such a destabilization of the microtubule cytoskeleton, which is reminiscent of microtubule changes induced after traumatic axon injury (Erez et al., 2007; Kleele et al., 2014), might mark the transition to more permanent structural axon damage and predispose affected axons to subsequent degeneration.

### Anti-Inflammatory and Anti-Oxidative Interventions Reverse Transport Deficits in Multiple Sclerosis Models

Our results show that transport deficits can be initiated in morphologically normal axons with intact myelin, normal-appearing

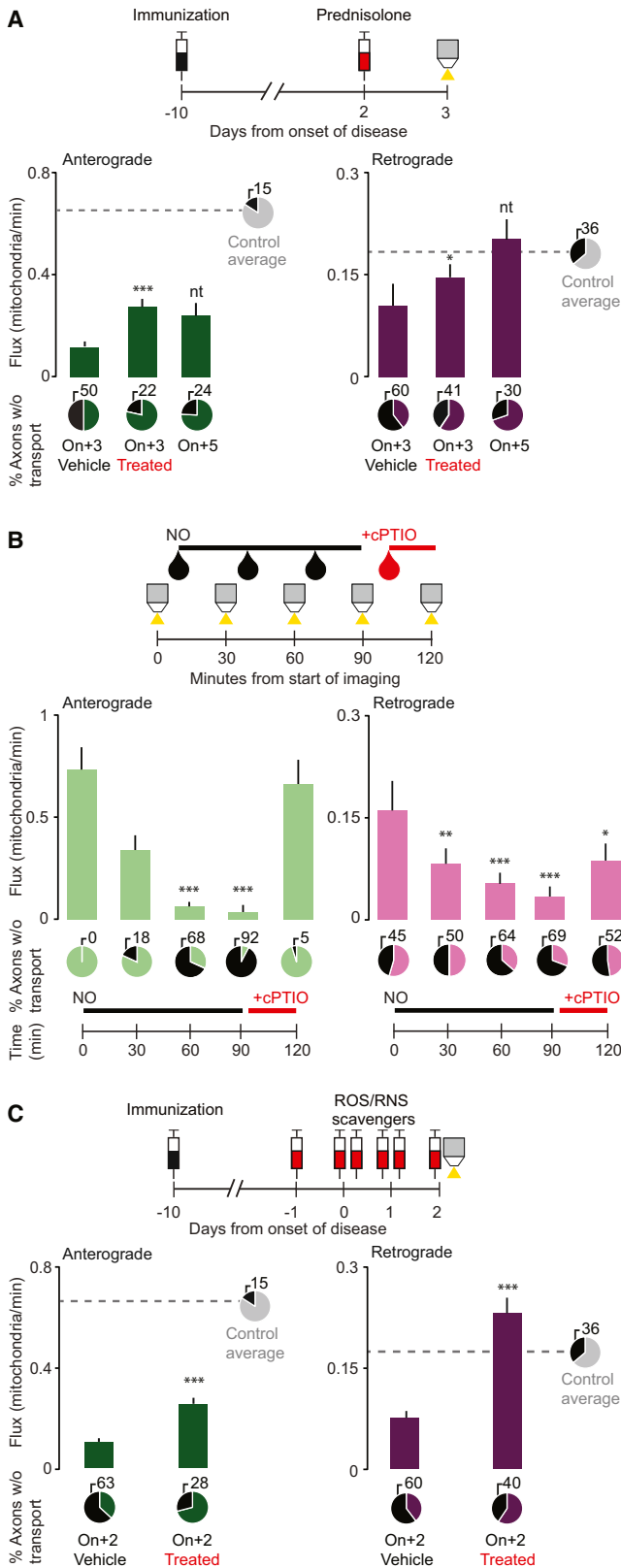


**Figure 4. Transport Deficits Can Be Reversed by Glucocorticoid Treatment and Redox Scavenging**

(A) Schematic diagram (top) of the treatment of *Thy1-YFP-16* × *Thy1-MitoCFP-P* mice with a single dose (20 mg/kg) of methylprednisolone 2 days after onset of EAE followed by in vivo imaging the following day. Bottom: quantification of anterograde and retrograde mitochondrial flux in EAE mice treated with vehicle (“Vehicle”) or methylprednisolone (“Treated”) compared to untreated EAE mice imaged at 5 days after onset ( $n = 33\text{--}79$  stage 0 axons with normally shaped mitochondria from 3–5 mice per group; flux in methylprednisolone-treated mice compared to flux in vehicle-treated mice with Mann-Whitney test; “nt,” not tested). Pie charts represent the percentage of axons where no transport was seen (black slice, percentage indicated above). As a comparison, dashed gray line and gray pie chart represent average flux and percentage of axons with no transport measured in healthy mice as shown in Figure 1. (B) Schematic diagram (top) of bath application of the nitric oxide donor at a dose that does not induce axonal degeneration (Spermine NONOate, 8 mM; “NO”) and the NO scavenger cPTIO (500  $\mu\text{M}$ ; “+cPTIO”) to the exposed lumbar spinal cord of control *Thy1-YFP-16* × *Thy1-MitoCFP-P* mice. Donor was replenished with fresh stock following each imaging time point to ensure continuous release of NO. Bottom: quantification of anterograde and retrograde flux of mitochondria at different time points after NO donor application ( $n = 22$  axons from 5 mice; flux compared to initial time point, “0,” by Kruskal-Wallis test followed by Dunn’s Multiple Comparison test). Pie charts represent the percentage of axons where no transport was seen (black slice, percentage indicated above). (C) Schematic diagram (top) of the treatment of *Thy1-YFP-16* × *Thy1-MitoCFP-P* mice with i.p. injections of vehicle (“Vehicle”) or a ROS/RNS scavenger cocktail (“Treated”) beginning at weight loss (“–1”), and continued every 12 hr, until 2 days after onset of EAE. Bottom: quantification of mitochondrial flux measured at 2 days after onset with accompanying pie charts of the percentage of axons without transport ( $n = 156\text{--}158$  stage 0 axons with normally shaped mitochondria from 8 mice per group; flux compared to flux in vehicle-treated mice with Mann-Whitney test). As a comparison, dashed gray line and gray pie chart represent average flux and percentage of axons with no transport measured in healthy mice as shown in Figure 1. All graphs show mean + SEM; \* $p < 0.05$ ; \*\* $p < 0.01$ ; \*\*\* $p < 0.001$ .

cargos, and unaltered microtubule tracks. Hence, transport deficits appear to represent an early state of inflammation-induced axonal “dysfunction” rather than a later sequel of structural alterations. This suggests that transport deficits could reverse once the underlying inflammatory driving force subsides. Indeed, transport deficits started to recover within a few days after the peak of EAE in the acute model. This recovery could be accelerated by treating mice at the peak of their symptoms with a single dose of corticosteroids, an intervention that is commonly used to curb disease exacerbation in MS patients (Sellebjerg et al., 2005; Figure 4A). Next, we asked which inflammatory mediators could cause such reversible axonal dysfunction. Reactive oxygen species (ROS) and reactive nitrogen species (RNS) were previously shown to induce transport deficits in vitro (Stagi et al., 2005) and to initiate structural axon damage in vivo (Nikić et al., 2011). To follow the evolution of transport deficits over time after application of such reactive species, we repetitively measured axonal transport in individual spinal axons of healthy *Thy1-MitoCFP* mice for several hours. When we applied the NO donor, Spermine NONOate, at a dose that did not induce axonal degeneration, to the exposed spinal cord, organelle transport came to a complete halt within 90 min but could be restarted by application of the NO scavenger cPTIO (Figure 4B and Movie S4). To determine whether reactive species also contribute to the induction of transport deficits in neuroinflammatory lesions, we treated EAE mice with ROS/RNS scavengers. Indeed, therapeutic

neutralization of reactive species not only limits structural axon damage, as we have previously shown (Nikić et al., 2011), but also ameliorated axonal transport deficits (Figure 4C).

## DISCUSSION

By assaying the movement of individual axonal organelles in the spinal cord of living mice, we reveal widespread axonal transport deficits in neuroinflammatory lesions. Transport deficits affected diverse organelles such as mitochondria and peroxisomes and both anterograde and retrograde transport.

A number of surprising findings emerged from our study. First, transport deficits were already observed in normal-appearing and myelinated axons, indicating that demyelination is not required for initiation of inflammation-associated transport deficits. At the same time, in line with previous studies (Kiryu-See et al., 2010; Ohno et al., 2014), we find that demyelination modulates important aspects of axonal transport including the moving speed of anterograde organelle movement ( $0.31 \pm 0.03 \mu\text{m/s}$  in normal appearing myelinated axons versus  $0.49 \pm 0.03 \mu\text{m/s}$  in all normal appearing axons in EAE,  $n = 17\text{--}81$  mitochondria from 4–18 *Thy1-YFP-16* × *Thy1-MitoCFP-P* mice per group), as well as the density of stationary mitochondria ( $93\% \pm 6\%$  of control in normal appearing myelinated axons versus  $149\% \pm 5\%$  of control in all normal appearing axons in EAE,  $n = 30\text{--}128$  axons from 4–18 *Thy1-YFP-16* × *Thy1-MitoCFP-P* mice per group). It is thus likely that in neuroinflammatory lesions the final transport pattern reflects both the influences of inflammation and demyelination, the relative importance of which might shift as the disease advances. Second, transport deficits occurred before marked alterations of the ultrastructure or acetylation of microtubule tracks could be observed. Imaging of fluorescently labeled microtubule end-binding proteins further showed that the stability of microtubules was likewise unaltered in the initial stage of axonal dysfunction when transport deficits start to manifest. Third, transport deficits were strikingly reversible, both spontaneously and after intervention, suggesting that altered transport might be a suitable therapeutic target. Indeed, both a standard anti-inflammatory treatment, as well as a redox-scavenging protocol, efficiently reversed the transport deficit.

So how does inflammation cause reversible transport deficits? While multiple factors are likely to contribute, a number of observations point to alterations of motor engagement at the microtubules. First, we did not find any structural changes of axons, cargos, or tracks that correlated with transport deficits, making it unlikely that overt structural damage disrupts transport. Second, both mitochondria and peroxisomes, as well as anterograde and retrograde transport, are affected, making a primary interruption of organelle-specific linkers, such as Miro or Trak (Schwarz, 2013), or of specific motors, such as kinesins or dynein, unlikely. Finally, tracking of single organelles revealed that stop duration is dramatically increased in the inflamed spinal cord, suggesting a temporary disengagement of cargos from tracks. This notion is further supported by the increased density and content of mitochondria observed in EAE axons that suggest that moving mitochondria accumulate in the lesion area. Indeed, arrest of moving mitochondria (which are comparatively smaller than resting ones;

Misgeld et al., 2007 and data not shown) might explain the drop in the average mitochondrial volume observed in early stages of axon damage, but which later normalizes as axon damage progresses, perhaps due to mitochondrial fusion or local growth (relative mitochondrial volume:  $63\% \pm 1\%$  in normal appearing axons and  $97\% \pm 4\%$  in swollen axons in EAE,  $n = 397\text{--}1,361$  mitochondria from 3–4 *Thy1-YFP-16* × *Thy1-MitoCFP-S* mice per group). The organelle accumulations we found could thus be caused by local molecular alterations of microtubules that affect binding of different motor-cargo complexes. Indeed, the reduced severity and faster recovery of retrograde transport deficits we observed could be explained by the fact that dynein motors can circumvent such obstacles more efficiently than kinesins (Dixit et al., 2008). While we observe a more prominent impairment of the anterograde transport, it should be noted that in other neurological conditions, e.g., in a mouse model of hereditary spastic paraplegia, a selective accumulation of retrograde motor proteins and consequent disturbance of retrograde transport have been described (Edgar et al., 2004). Obstacles for organelle transport could in principle result from posttranslational modification and destabilization of microtubules, e.g., by tyrosination or deacetylation (Dunn et al., 2008; Reed et al., 2006). Our results, however, show no evidence for microtubule deacetylation and indicate that microtubule tyrosination as well as changes in microtubule dynamics primarily occur in the late stages of axon damage (Figures 3C–3E and Figure S5). An alternative cause for motor-to-track disruptions is the excessive attachment of microtubule-associated proteins (MAPs), which can competitively inhibit the binding of motors to microtubules (Dixit et al., 2008). Notably, MAPs can be targeted by reactive oxygen or nitrogen species either directly (Stroissnigg et al., 2007) or through activation of upstream kinases (Dias-Santagata et al., 2007). The quick reversal of NO donor-induced transport deficits that occurred after application of the NO scavenger cPTIO (Figure 4B) is compatible with the idea that reversible MAP modifications such as oxidation or phosphorylation mediate transport arrest.

Taken together, our data thus suggest that reactive species released by activated immune cells in neuroinflammatory lesions acutely induce transport disruptions by altering the attachment of motor/cargo complexes to microtubules. Notably, these transport deficits could be induced by NO donor doses that were lower than those that cause structural axon damage (Nikić et al., 2011). This dose dependence of structural versus functional axon impairments suggests that in an inflammatory lesion, there is a center where high doses of reactive species induce structural axon damage, surrounded by a larger “penumbra,” in which lower doses of such mediators cause transient axonal dysfunction. Consequently, when inflammation subsides, for example during remission of an acute neuroinflammatory lesion, transport recovers within days in the penumbral zone. The localized nature of the transport deficits we observe is underlined by our findings that within dorsal root axons that reside outside the CNS and are therefore not locally exposed to inflammation, anterograde flux is normal, while retrograde flux is significantly increased compared to control (Figure S1). The latter indicates that some cargoes reverse when confronted with a structural or functional barrier, similar to what occurs following traumatic axon transection (Misgeld et al., 2007). While transport deficits are thus locally induced,

they likely also affect organelle flux in axons both proximal and distal to the lesion area, which could further affect the transport rates measured in those axons that pass through several lesions. Still, when short-lasting, such transport deficits probably have no immediate detrimental consequences for affected axons (Figures S3C and S3D) and even structurally affected axons can recover during remission (Nikić et al., 2011). However, in situations in which inflammation persists, even at low levels, as in progressive MS and its models, transport deficits are perpetuated. As anterograde transport is predominantly affected, this limits the provision of vital organelles and ultimately results in “starvation” of distal axonal arbors (Figure S3). Ensuing axonal dystrophy would probably first manifest most distally at the synapse and follow a “dying-back” pattern (Coleman, 2005). Indeed, recent histopathological studies provide evidence for prominent synaptic pathology in progressive MS patients (Dutta et al., 2011; Mori et al., 2013). Preventing persistent transport deficits, e.g., by prolonged redox scavenging, might thus help to reverse transport-based axon dysfunction and thereby help to counteract emerging axonal dystrophy.

## EXPERIMENTAL PROCEDURES

### Transgenic Animals

In *Thy1-YFP-16* (Jackson Laboratory strain designation: *Tg(Thy1-YFP)16Jrs/J*), *Thy1-OPF-3*, and *Thy1-CFP-5* mice, a large proportion of axons is labeled, while the *Thy1-GFP-S* line labels only a small subset (Brill et al., 2011; Feng et al., 2000). In *Thy1-MitoCFP-P* and *Thy1-MitoCFP-S* (Jackson Laboratory strain designation: *Tg(Thy1-CFP/COX8A)S2Lich/J*) mice, a mitochondrial import sequence directs CFP expression selectively to neuronal mitochondria (Misgeld et al., 2007). To study mitochondria transport rates in the acute EAE model, we used double-transgenic *Thy1-YFP-16* × *Thy1-MitoCFP-P* mice. To study mitochondrial transport in chronic EAE, we obtained BiozziABH mice from Harlan Laboratories (strain designation BiozziABH/RijHsd) and crossed them with *Thy1-MitoCFP-P* or *Thy1-MitoCFP-S* mice. F1 mice were used for analysis. *Thy1-YFP-EB3-J045* mice, which express a YFP-tagged version of the plus-end binding protein EB3 selectively in neurons (Kleele et al., 2014) were used for in vivo microtubule “comet” analysis and crossed with *Thy1-OPF-3* mice to visualize axons or *Thy1-MitoCFP-P* for concomitant imaging of mitochondria.

See details of the generation of peroxisome mice, in vivo microscopy and analysis, tissue preparation and analysis, surgical procedures, and virus production in Supplemental Experimental Procedures.

### Statistical Analysis

All data sets were tested for normal distribution with the D’Agostino-Pearson normality test using GraphPad Prism software. If the data sets failed said test, a nonparametric test was chosen to compare the significance of means between groups (Mann-Whitney test for two samples, Kruskal-Wallis test followed by Dunn’s Multiple Comparison test for more than two samples). The chosen statistical test is indicated in each accompanying figure legend along with its corresponding p value if applicable.

## SUPPLEMENTAL INFORMATION

Supplemental Information includes Supplemental Experimental Procedures, five figures, and four movies and can be found with this article online at <http://dx.doi.org/10.1016/j.neuron.2014.11.006>.

## AUTHOR CONTRIBUTIONS

M.K., T.M., and C.D.S. conceived the experiments. C.D.S., M.K., and T.M. performed imaging experiments and image analysis. C.D.S., N.E.W., A.L., I.N.,

D.M., and F.M.B. contributed to histological analysis. T.K., R.N., L.G., and P.M. generated and characterized transgenic mouse lines. D.B. and C.D.S. performed electron microscopy analysis. T.M., M.K., and C.D.S. wrote the paper.

## ACKNOWLEDGMENTS

We would like to thank A. Schmalz, M. Adrian, Y. Hufnagel, and K. Wullmann for excellent technical assistance, D. Matzek, M. Budak, N. Budak, and L. Marinković for animal husbandry. We thank D. Crane (Griffith University, Brisbane) for the gift of anti-PEX14 antibody and R. Hohfeld for critical reading of the manuscript. We thank E. Ruthazer (McGill University, Montreal) for pointing out the CANDLE denoising algorithm. Work in M.K.’s laboratory is financed through grants from the Deutsche Forschungsgemeinschaft (DFG; Transregio 128), the German Federal Ministry of Research and Education (BMBF; Competence Network Multiple Sclerosis), the European Research Council under the European Union’s Seventh Framework Program (FP/2007-2013; ERC Grant Agreement n. 310932), the Hertie-Foundation and the “Verein Therapiefor-schung für MS-Kranke e.V..” T.M. is supported by the Center for Integrated Protein Science (Munich, EXC 114), the European Research Council under the European Union’s Seventh Framework Program (FP/2007-2013; ERC Grant Agreement n. 616791), and the German Center for Neurodegenerative Disease (DZNE Munich). F.M.B. is supported by an independent group leader award of the BMBF. F.M.B., M.K., and T.M. are supported by the Munich Center for Systems Neurology (SyNergy; EXC 1010). M.K. and T.M. are supported by the DFG Priority Program 1710. F.M.B., L.G., and T.M. are supported by the DFG-funded collaborative research center 870. D.M. holds a stipendiary professorship of the Swiss National Science Foundation (No. PP00P3\_152928) and is supported by the Klaus-Tschira Foundation and the Gebert-Rüf Foundation. C.D.S., T.K., and P.M. were supported by the Graduate School of Technische Universität München (TUM-GS).

Accepted: October 31, 2014

Published: November 26, 2014

## REFERENCES

- Baloh, R.H., Schmidt, R.E., Pestronk, A., and Milbrandt, J. (2007). Altered axonal mitochondrial transport in the pathogenesis of Charcot-Marie-Tooth disease from mitofusin 2 mutations. *J. Neurosci.* 27, 422–430.
- Brill, M.S., Lichtman, J.W., Thompson, W., Zuo, Y., and Misgeld, T. (2011). Spatial constraints dictate glial territories at murine neuromuscular junctions. *J. Cell Biol.* 195, 293–305.
- Coleman, M. (2005). Axon degeneration mechanisms: commonality amid diversity. *Nat. Rev. Neurosci.* 6, 889–898.
- d’Ydewalle, C., Krishnan, J., Chiheb, D.M., Van Damme, P., Irobi, J., Kozikowski, A.P., Vanden Berghe, P., Timmerman, V., Robberecht, W., and Van Den Bosch, L. (2011). HDAC6 inhibitors reverse axonal loss in a mouse model of mutant HSPB1-induced Charcot-Marie-Tooth disease. *Nat. Med.* 17, 968–974.
- Davalos, D., Lee, J.K., Smith, W.B., Brinkman, B., Ellisman, M.H., Zheng, B., and Akassoglou, K. (2008). Stable in vivo imaging of densely populated glia, axons and blood vessels in the mouse spinal cord using two-photon microscopy. *J. Neurosci. Methods* 169, 1–7.
- Denton, K.R., Lei, L., Grenier, J., Rodionov, V., Blackstone, C., and Li, X.J. (2014). Loss of spastin function results in disease-specific axonal defects in human pluripotent stem cell-based models of hereditary spastic paraplegia. *Stem Cells* 32, 414–423.
- Dias-Santagata, D., Fulga, T.A., Duttaroy, A., and Feany, M.B. (2007). Oxidative stress mediates tau-induced neurodegeneration in *Drosophila*. *J. Clin. Invest.* 117, 236–245.
- Dixit, R., Ross, J.L., Goldman, Y.E., and Holzbaur, E.L. (2008). Differential regulation of dynein and kinesin motor proteins by tau. *Science* 319, 1086–1089.
- Dunn, S., Morrison, E.E., Liverpool, T.B., Molina-Paris, C., Cross, R.A., Alonso, M.C., and Peckham, M. (2008). Differential trafficking of Kif5c on tyrosinated and detyrosinated microtubules in live cells. *J. Cell Sci.* 121, 1085–1095.

- Dutta, R., Chang, A., Doud, M.K., Kidd, G.J., Ribaud, M.V., Young, E.A., Fox, R.J., Staugaitis, S.M., and Trapp, B.D. (2011). Demyelination causes synaptic alterations in hippocampi from multiple sclerosis patients. *Ann. Neurol.* *69*, 445–454.
- Ebbing, B., Mann, K., Starosta, A., Jaud, J., Schöls, L., Schüle, R., and Woehlke, G. (2008). Effect of spastic paraplegia mutations in KIF5A kinesin on transport activity. *Hum. Mol. Genet.* *17*, 1245–1252.
- Edgar, J.M., McLaughlin, M., Yool, D., Zhang, S.C., Fowler, J.H., Montague, P., Barrie, J.A., McCulloch, M.C., Duncan, I.D., Garbern, J., et al. (2004). Oligodendroglial modulation of fast axonal transport in a mouse model of hereditary spastic paraplegia. *J. Cell Biol.* *166*, 121–131.
- Erez, H., Malkinson, G., Prager-Khoutorsky, M., De Zeeuw, C.I., Hoogenraad, C.C., and Spira, M.E. (2007). Formation of microtubule-based traps controls the sorting and concentration of vesicles to restricted sites of regenerating neurons after axotomy. *J. Cell Biol.* *176*, 497–507.
- Feng, G., Mellor, R.H., Bernstein, M., Keller-Peck, C., Nguyen, Q.T., Wallace, M., Nerbonne, J.M., Lichtman, J.W., and Sanes, J.R. (2000). Imaging neuronal subsets in transgenic mice expressing multiple spectral variants of GFP. *Neuron* *28*, 41–51.
- Hurd, D.D., and Saxton, W.M. (1996). Kinesin mutations cause motor neuron disease phenotypes by disrupting fast axonal transport in *Drosophila*. *Genetics* *144*, 1075–1085.
- Janke, C. (2014). The tubulin code: molecular components, readout mechanisms, and functions. *J. Cell Biol.* *206*, 461–472.
- Kiryu-Seo, S., Ohno, N., Kidd, G.J., Komuro, H., and Trapp, B.D. (2010). Demyelination increases axonal stationary mitochondrial size and the speed of axonal mitochondrial transport. *J. Neurosci.* *30*, 6658–6666.
- Kleele, T., Marinković, P., Williams, P.R., Stern, S., Weigand, E.E., Engerer, P., Naumann, R., Hartmann, J., Karl, R.M., Bradke, F., et al. (2014). An assay to image neuronal microtubule dynamics in mice. *Nat. Commun.* *5*, 4827.
- LaMonte, B.H., Wallace, K.E., Holloway, B.A., Shelly, S.S., Ascaño, J., Tokito, M., Van Winkle, T., Howland, D.S., and Holzbaur, E.L. (2002). Disruption of dynein/dynactin inhibits axonal transport in motor neurons causing late-onset progressive degeneration. *Neuron* *34*, 715–727.
- Lassmann, H., van Horssen, J., and Mahad, D. (2012). Progressive multiple sclerosis: pathology and pathogenesis. *Nat Rev Neurol* *8*, 647–656.
- Millecamps, S., and Julien, J.P. (2013). Axonal transport deficits and neurodegenerative diseases. *Nat. Rev. Neurosci.* *14*, 161–176.
- Misgeld, T., Kerschensteiner, M., Bareyre, F.M., Burgess, R.W., and Lichtman, J.W. (2007). Imaging axonal transport of mitochondria in vivo. *Nat. Methods* *4*, 559–561.
- Mori, F., Rossi, S., Piccinin, S., Motta, C., Mango, D., Kusayanagi, H., Bergami, A., Studer, V., Nicoletti, C.G., Buttari, F., et al. (2013). Synaptic plasticity and PDGF signaling defects underlie clinical progression in multiple sclerosis. *J. Neurosci.* *33*, 19112–19119.
- Nikić, I., Merkler, D., Sorbara, C., Brinkoetter, M., Kreutzfeldt, M., Bareyre, F.M., Brück, W., Bishop, D., Misgeld, T., and Kerschensteiner, M. (2011). A reversible form of axon damage in experimental autoimmune encephalomyelitis and multiple sclerosis. *Nat. Med.* *17*, 495–499.
- Ohno, N., Chiang, H., Mahad, D.J., Kidd, G.J., Liu, L., Ransohoff, R.M., Sheng, Z.H., Komuro, H., and Trapp, B.D. (2014). Mitochondrial immobilization mediated by syntrophin facilitates survival of demyelinated axons. *Proc. Natl. Acad. Sci. USA* *111*, 9953–9958.
- Reed, N.A., Cai, D., Blasius, T.L., Jih, G.T., Meyhofer, E., Gaertig, J., and Verhey, K.J. (2006). Microtubule acetylation promotes kinesin-1 binding and transport. *Curr. Biol.* *16*, 2166–2172.
- Romanelli, E., Sorbara, C.D., Nikić, I., Dagkalis, A., Misgeld, T., and Kerschensteiner, M. (2013). Cellular, subcellular and functional in vivo labeling of the spinal cord using vital dyes. *Nat. Protoc.* *8*, 481–490.
- Schwarz, T.L. (2013). Mitochondrial trafficking in neurons. *Cold Spring Harb. Perspect. Biol.* *5*, 5.
- Sellebjerg, F., Barnes, D., Filippini, G., Midgard, R., Montalban, X., Rieckmann, P., Selmaj, K., Visser, L.H., and Sørensen, P.S.; EFNS Task Force on Treatment of Multiple Sclerosis Relapses (2005). EFNS guideline on treatment of multiple sclerosis relapses: report of an EFNS task force on treatment of multiple sclerosis relapses. *Eur. J. Neurol.* *12*, 939–946.
- Stagi, M., Ditttrich, P.S., Frank, N., Iliev, A.I., Schwille, P., and Neumann, H. (2005). Breakdown of axonal synaptic vesicle precursor transport by microglial nitric oxide. *J. Neurosci.* *25*, 352–362.
- Stroissnigg, H., Tranciková, A., Descovich, L., Fuhrmann, J., Kutschera, W., Kostan, J., Meixner, A., Nothias, F., and Propst, F. (2007). S-nitrosylation of microtubule-associated protein 1B mediates nitric-oxide-induced axon retraction. *Nat. Cell Biol.* *9*, 1035–1045.
- Trapp, B.D., and Nave, K.A. (2008). Multiple sclerosis: an immune or neurodegenerative disorder? *Annu. Rev. Neurosci.* *31*, 247–269.
- Vergo, S., Craner, M.J., Etzensperger, R., Atfield, K., Friese, M.A., Newcombe, J., Esiri, M., and Fugger, L. (2011). Acid-sensing ion channel 1 is involved in both axonal injury and demyelination in multiple sclerosis and its animal model. *Brain* *134*, 571–584.
- Witte, M.E., Bø, L., Rodenburg, R.J., Belien, J.A., Musters, R., Hazes, T., Wintjes, L.T., Smeitink, J.A., Geurts, J.J., De Vries, H.E., et al. (2009). Enhanced number and activity of mitochondria in multiple sclerosis lesions. *J. Pathol.* *219*, 193–204.
- Witte, M.E., Mahad, D.J., Lassmann, H., and van Horssen, J. (2014). Mitochondrial dysfunction contributes to neurodegeneration in multiple sclerosis. *Trends Mol. Med.* *20*, 179–187.